Torque ripple reduction for 12-stator/10-rotor-pole variable flux reluctance machines by rotor skewing or rotor teeth non-uniformity

Torque Ripple Reduction for 12-stator/10-rotor-pole Variable Flux Reluctance Machines by Rotor Skewing or Rotor Teeth Non-uniformity

J. Bao, B.L.J. Gysen, K. Boynov, J.J.H Paulides and E.A. Lomonova
Department of Electrical Engineering, Eindhoven University of Technology, Eindhoven, the Netherlands

Variable flux reluctance machines are interesting candidates to substitute permanent-magnet synchronous machines in many applications. However, they suffer from large torque ripple. In this paper two methods, stepped rotor skewing and rotor teeth non-uniformity are researched to reduce the torque ripple of 12/10 (stator/rotor pole ratio) variable flux reluctance machines. Based on semi-analytic results and finite element simulations, the effectiveness of these two methods is validated in both non-saturated and saturated machines.

***Index Terms*—Variable flux reluctance machine, torque ripple reduction, skewing.**

I. Introduction

VARIABLE flux reluctance machines (VFRMs) with electrically DC-excited field, have been researched in recent years as candidates for replacing permanent-magnet synchronous machines due to the price fluctuation of rare-earth permanent magnets [1], [2]. This kind of machine has a robust rotor structure, wide speed range and is easy to manufacture, [3]. However, for applications requiring low noise or smooth torque, torque ripple is an issue that needs to be investigated, [5], [6].

Different methods for torque ripple reduction have been analyzed for VFRMs. In [4], harmonic injection in the DC-field windings is introduced. In [5], different skewing and tooth chamfering methods are briefly introduced. However, derivation of the skewing angle in non-saturated and saturated machines is not explained. In this paper, sources of torque ripple in 12/10 VFRMs are analyzed, and two methods are investigated for torque ripple reduction. In section II, the harmonics in the inductances are explained and their corresponding contributions to torque ripple are derived. Afterwards, in section III and IV, the methods of stepped rotor skewing and rotor teeth non-uniformity are given based on the results presented in section II. For each method, dependence of torque ripple and average torque on the skewing angle is presented and finally, conclusions are given.

II. Torque ripple analysis

The geometry of a 12/10 VFRM is shown in Fig. 1. The average torque and torque ripple are dependent on the variation of inductances. In VFRM, there are basically four types of inductances: self inductance of DC-field windings (L_f); mutual inductances between field and armature windings of phase a, b and c (M_{fa}, M_{fb} and M_{fc}); self inductances of armature windings (L_a, L_b and L_c) and mutual inductances between armature windings (M_{ab}, M_{bc} and M_{ac}). Neglecting saturation, the contribution of these inductances to the eletromagnetic torque, $T_{em,tot}$, is derived using the virtual work method, [7]

Corresponding author: J. Bao (email: j.bao@tue.nl)

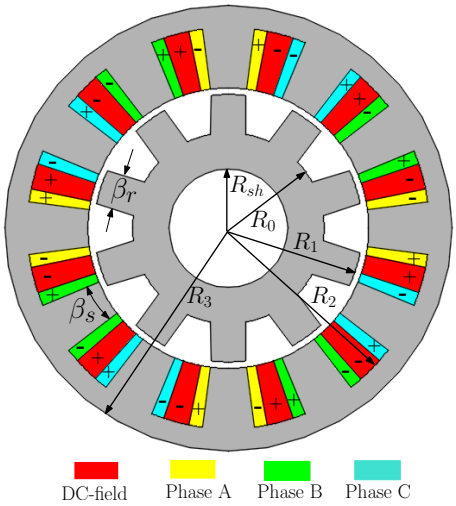

Fig. 1. Geometry of a 12/10 VFRM without skewing.

$$\begin{aligned} T_{em,tot} &= T_{ff} + T_{f,ph} + T_{l,ph} + T_{m,ph} \\ &= \left(\frac{1}{2} I_f^2 \frac{dL_f}{d\theta}\right) + \left(I_f i_a \frac{dM_{fa}}{d\theta} + I_f i_b \frac{dM_{fb}}{d\theta} + I_f i_c \frac{dM_{fc}}{d\theta}\right) \\ &+ \left(\frac{1}{2} i_a^2 \frac{dL_a}{d\theta} + \frac{1}{2} i_b^2 \frac{dL_b}{d\theta} + \frac{1}{2} i_c^2 \frac{dL_c}{d\theta}\right) \\ &+ \left(i_a i_b \frac{dM_{ab}}{d\theta} + i_a i_c \frac{dM_{ac}}{d\theta} + i_b i_c \frac{dM_{bc}}{d\theta}\right), \end{aligned} \tag{1}$$

where torque components, T_{ff}, $T_{f,ph}$, $T_{l,ph}$ and $T_{m,ph}$ represent the torque induced by the self inductance of DC-field windings, mutual inductances between field and armature windings, self inductances of armature windings and mutual inductances of armature windings, respectively; while i_a, i_b, i_c and I_f are the armature and field currents, respectively. To

TABLE I
Dimensions of the VFRM in this paper.

Parameter	Description	value
g	Airgap length	0.5 mm
l_{sk}	Stack length	87.5 mm
R_{sh}	Shaft radius	17 mm
R_0	Rotor inner radius	30 mm
R_1	Rotor outer radius	42 mm
R_2	Radius to stator slot inner side	62.5 mm
R_3	Stator outer radius	70 mm
β_s	Stator tooth arc	15°
β_r	Rotor tooth arc	15°
N_{AC}	Number of turns per AC coil	10
N_{DC}	Number of turns per DC coil	40

analyze the inductances and torque, a 2D finite element model (FEM) is created with the dimensions listed in TABLE I using the package of Altair Flux2D. The torque components are calculated using the following steps:

Step 1) T_{ff} is calculated by merely applying the field current;
Step 2) $T_{l,ph}$ is the resultant value of the torques that obtained by exciting phase a, b and c individually;
Step 3) The value of $(T_{l,ph} + T_{m,ph})$ is calculated by exciting the three-phase armature currents simultaneously, afterwards by subtracting the value of $T_{l,ph}$, $T_{m,ph}$ is obtained;
Step 4) $T_{em,tot}$ is simulated by exciting both the field and armature currents simultaneously, and $T_{f,ph}$ is derived by subtracting $(T_{ff} + T_{l,ph} + T_{m,ph})$ from $T_{em,tot}$.

Using the steps introduced above, the calculated spectra of inductances and torque components are shown in Fig. 2 and Fig. 3. As it can be seen, the integer multiple of the 6^{th} harmonic are dominant in L_f, since the distribution winding factors of these harmonics are unitary. Meanwhile, the 5^{th} harmonic dominates in M_{fa}. To find out the relationship between the torque components and the harmonics of inductances, the following expressions are derived from (1),

$$T_{ff} = \sum_{n=1}^{\infty} -\frac{1}{2} P_r n \hat{L}_{fn} \sin\left(n\theta_e + \theta_{fn}\right) I_f^2, \tag{2}$$

$$\begin{aligned} T_{f,ph} = & \sum_{n=3k+1}^{\infty} -\frac{3nP_r M_{fan} I_f \hat{I}_a}{2} \cos\left[(n-1)\theta_e + \theta_{fan}\right] \\ & + \sum_{n=3k+2}^{\infty} \frac{3nP_r \hat{M}_{fan} I_f \hat{I}_a}{2} \cos\left[(n+1)\,\theta_e + \theta_{fan}\right], \end{aligned} \tag{3}$$

where n is the n^{th} harmonic, θ_e is the rotor position in electric angle, P_r is the number of rotor poles, $\hat{I}_a$ is the amplitude of i_a, and $\hat{L}_{fn}$, $\hat{M}_{fan}$, θ_{fn} and θ_{fan} are the amplitudes and initial angles in the n^{th} harmonic of L_f and M_{fa}, respectively. It is worth mentioning that the expressions of $T_{l,ph}$ and $T_{m,ph}$ are not introduced is this paper, since these two components generally make modest contributions to the total torque ripple as illustrated in Fig. 3. The reason is that to achieve a high power factor, the magnetomotive force of the field current has a relatively large magnitude compared to that of the armature current.

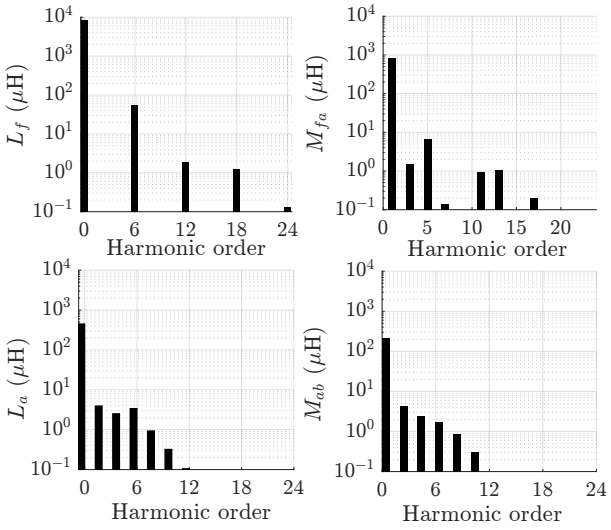

Fig. 2. Spectra of harmonics in inductances.

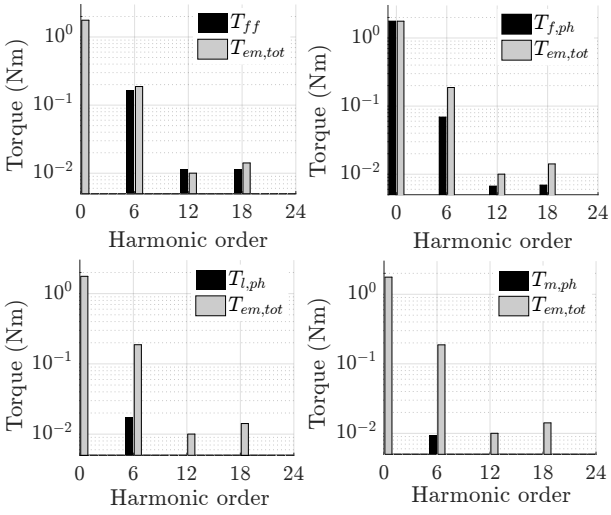

Fig. 3. Spectra of torque components in comparison with total electromagnetic torque when I_f = 10 A and $\hat{I}_a$ = $10\sqrt{2}$ A.

For verification, the torque components predicted by the equations are compared with the results obtained from FEA. The waveforms are presented in Fig. 4. The results show good agreement, that the difference between the values obtained by the two methods is within 0.8%.

According to (2) and (3), the 6^{th} harmonic in T_{ff} and $T_{f,ph}$ are expressed as,

$$T_{ff6} = -3\hat{L}_{f6} P_r I_f^2 \sin(6\theta_e + \theta_{f6}), \tag{4}$$

$$\begin{aligned} T_{f,ph6} &= \frac{15}{2} P_r \hat{M}_{fa5} I_f \hat{I}_a \cos\left(6\theta_e + \theta_{fa5}\right) \\ &\quad - \frac{21}{2} P_r \hat{M}_{fa7} I_f \hat{I}_a \cos\left(6\theta_e + \theta_{fa7}\right) \\ &\approx \frac{15}{2} P_r \hat{M}_{fa5} I_f \hat{I}_a \cos\left(6\theta_e + \theta_{fa5}\right) \end{aligned} \tag{5}$$

where $\hat{L}_{f6}$ and θ_{f6} are the amplitude and initial angle of the 6^{th} harmonic in L_f, and $\hat{M}_{fa5}$, $\hat{M}_{fa7}$, θ_{fa5} and θ_{fa7} are the amplitudes and initial angles of the 5^{th} and 7^{th}

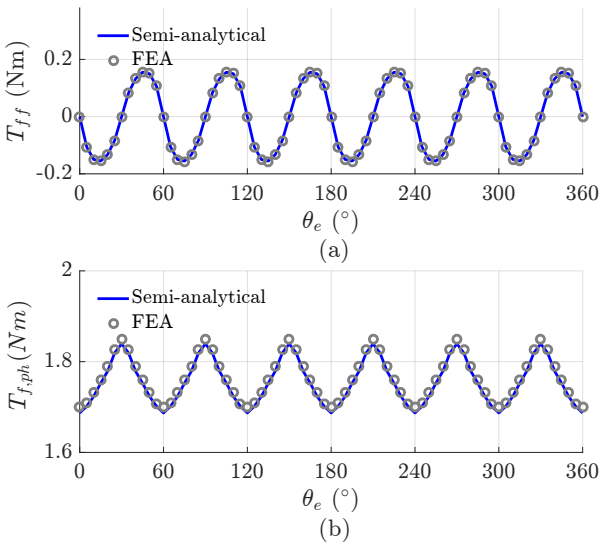

Fig. 4. Comparison of torque waveforms obtained by using semi-analytical model and FEA when I_f = 10 A and $\hat{I}_a = 10\sqrt{2}$ A.

harmonics in M_{fa}, respectively. Since the magnitude of $\hat{M}_{fa7}$ is significantly smaller than $\hat{M}_{fa5}$, the influence of $\hat{M}_{fa7}$ on $T_{f,ph6}$ can be ignored. As a result, the large magnitudes of $\hat{L}_{f6}$ and $\hat{M}_{fa5}$ lead to a large 6^{th} harmonic in T_{ff} and $T_{f,ph}$, respectively, as can be seen in Fig. 3.

III. Stepped Rotor Skewing

Rotor skewing topology is analyzed in this section. Compared to continuous skewing, stepped rotor skewing simplifies the manufacturing process and reduces cost, [8]. The analysis in this paper focuses on the geometry with two modules, since for more modules the working principle is the same.

The geometry of the stepped skewing rotor is shown in Fig. 5(a). The laminations in the front and rear modules are aligned, however, between the two modules, there is a skewing angle, θ_{sk}. Assume the front half of the machine generates a back-emf of,

$$E_{front} = \hat{E}\sin(P_r\omega_r t). \tag{6}$$

where ω_r is the mechanical rotational speed and $\hat{E}$ is the amplitude of the fundamental back-emf. The back-emf of the rear half of the machine is accordingly

$$E_{rear} = \hat{E}\sin(P_r\omega_r t + \theta_{sk}). \tag{7}$$

The resultant back-emf is therefore

$$E_{tot} = 2\hat{E}\sin\left(P_r\omega_r t + \frac{P_r\theta_{sk}}{2}\right)\cos\left(\frac{P_r\theta_{sk}}{2}\right). \tag{8}$$

The armature current should be in phase with the back-emf to reach the maximum average torque. It means the sinusoidal current reaches zero when the centerline of the two modules aligns with the stator tooth, as shown in Fig. 5(b). As such, the ratio of the average torque in a skewed machine to the average torque in an un-skewed machine is

$$\frac{T'_{ave}}{T_{ave}} = \cos\left(\frac{P_r\theta_{sk}}{2}\right). \tag{9}$$

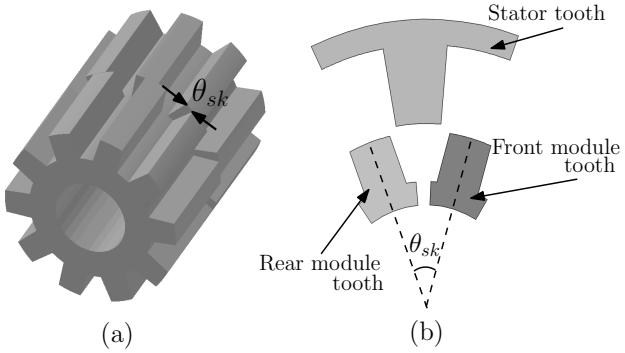

Fig. 5. (a) 3D geometry of a stepped skewing rotor with two modules and (b) position when armature current is zero.

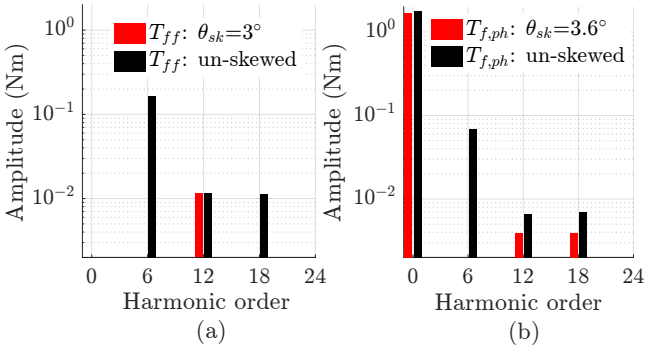

Fig. 6. (a) Spectrum of T_{ff} when $\theta_{sk} = 3°$ and (b) spectrum of $T_{f,ph}$ when $\theta_{sk} = 3.6°$.

A. Effect of the method for non-saturated machines

First the influence of skewing is analyzed in a non-saturated machine. To simplify the simulation, the two modules are represented by two 2D un-skewed machines whose rotors are relatively displaced by θ_{sk}, [9]. The 3D effect is not considered.

As explained in section II, the torque ripple is mainly composed of the 6^{th} harmonic in T_{ff} and $T_{f,ph}$, and the expressions are derived as (4) - (5) for an un-skewed machine. With skewing, the expressions become

$$\begin{aligned} T_{ff6} = &-\frac{3}{2}\hat{L}_{f6}P_r I_f^2\left[\sin\left(6\theta_e + \theta_{f6} - 3P_r\theta_{sk}\right)\right. \\ &\left.+\sin\left(6\theta_e + \theta_{f6} + 3P_r\theta_{sk}\right)\right], \end{aligned} \tag{10}$$

$$\begin{aligned} T_{f,ph6} \approx &\frac{15P_r\hat{M}_{fa5}I_f\hat{I}_a}{4}\left[\cos\left(6\theta_e + \theta_{fa5} - 2.5P_r\theta_{sk}\right)\right. \\ &\left.+\cos\left(6\theta_e + \theta_{fa5} + 2.5P_r\theta_{sk}\right)\right]. \end{aligned} \tag{11}$$

According to (10) - (11), T_{ff6} and $T_{f,ph6}$ can be canceled out when $\theta_{sk} = 3°$ and $\approx 3.6°$, respectively. This is verified by the spectra in Fig. 6, which shows the elimination of T_{ff6} and $T_{f,ph6}$ with a properly selected θ_{sk}.

For different dimensions, e.g. rotor tooth arc β_r, the contributions of T_{ff6} and $T_{f,ph6}$ to the total torque ripple vary. According to the previous analysis, if T_{ff6} dominates in an un-skewed structure, it is preferred to make θ_{sk} close to 3°, so that T_{ff6} is eliminated. On the contrary, if $T_{f,ph6}$ dominates in an un-skewed structure, θ_{sk} is preferred to be close to 3.6° to suppress $T_{f,ph6}$.

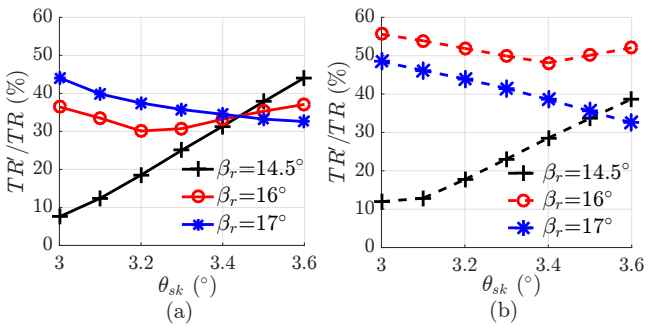

Fig. 7. Ratio of torque ripple in a skewed machine to torque ripple in an un-skewed machine when it is (a) non-saturated and (b) saturated.

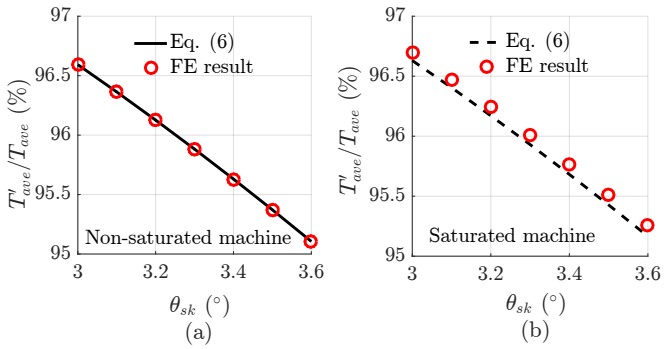

Fig. 8. Ratio of the average torque in a skewed machine to the average torque in an un-skewed machine ($\beta_r = 16°$) when it is (a) non-saturated and (b) saturated.

To verify this, rotor tooth arc is varied to obtain different values of T_{ff6} and $T_{f,ph6}$ (T_{ff6} is $\gg$, $\approx$, $\ll T_{f,ph6}$ when β_r is 14.5°, 16° and 17°, respectively). The ratio of torque ripple in a skewed machine to torque ripple in an un-skewed machine, TR'/TR, is simulated for different θ_{sk}. The obtained relationship is shown in Fig. 7(a). (In this paper, torque ripple is defined as the difference in maximum and minimum torque over one complete electric period). As can be seen, for β_r equals to 14.5° and 17°, the torque ripple is the smallest when θ_{sk} is close to 3° and 3.6°, respectively.

Additionally, the relationship between average torque and θ_{sk} is shown in Fig. 8(a). Both the values obtained by calculation using (6) and simulation in FEM are presented. As can be seen, the analytic result is in agreement with the FE result. (Since the value of β_r almost does not influence the average torque, merely the simulation result for $\beta_r = 16°$ is presented.)

B. Effect of the method for saturated machines

Saturation changes both the magnitudes and phases of inductances, therefore, the relationship between the torque components may alter significantly between non-saturated and saturated machines. As a result, it influences the relationship between the torque ripple and skewing angle. Such effect can be seen in Fig. 7(b) for $\beta_r = 16°$. On the other hand, saturation almost does not change the relationship between the average torque and θ_{sk}, as can be seen in Fig. 8(a) and Fig. 8(b).

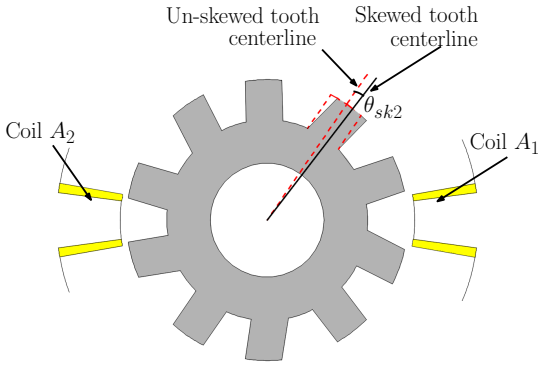

Fig. 9. Geometry of a rotor with non-uniformly distributed teeth.

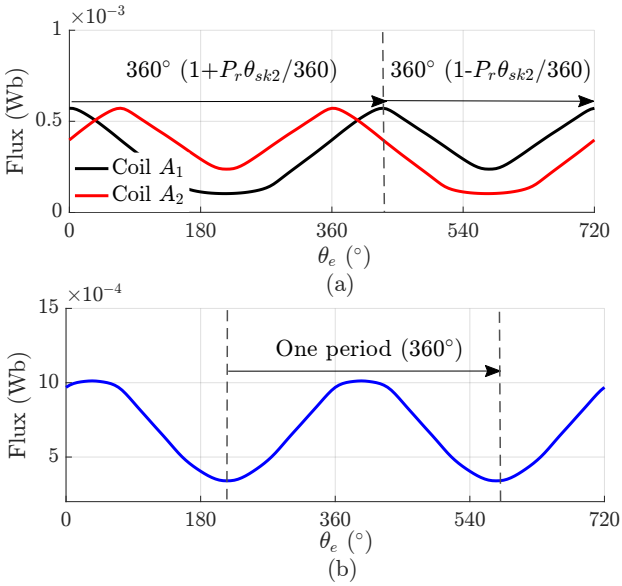

Fig. 10. (a) Flux of coil A_1 and A_2 in Fig. 9 and (b) resultant flux of the two coils.

Above all, the method of stepped rotor skewing works effectively for torque ripple reduction in both saturated and non-saturated machines.

IV. Rotor Teeth Non-Uniformity

As explained in section III, the working principle of the rotor skewing is to generate opposing torque ripple in different modules, therefore to reduce the resultant torque ripple. In this section, a method with a different working principle is analyzed. The geometry is shown in Fig. 9, where every other rotor tooth is skewed and the skewing angle remains the same along the stack length, [5].

The flux of one coil reaches maximum when a rotor tooth aligns with the corresponding stator tooth, and reaches minimum when they un-align. With a skewing angle of θ_{sk2}, the flux of two coils is shown in Fig. 10. As can be seen, the frequency of the flux of a single coil is half of the electric frequency. However, the sum of the two has the same period as an un-skewed structure. By properly tuning θ_{sk2}, the harmonics in the resultant flux are attenuated.

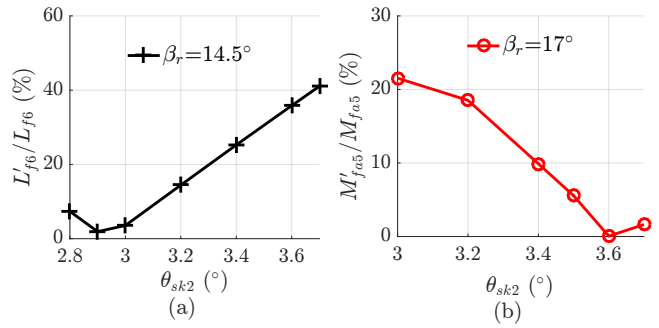

Fig. 11. Ratio of (a) $\hat{L}_{f6}$ and (b) $\hat{M}_{fa5}$ in a skewed machine to a non-skewed machine.

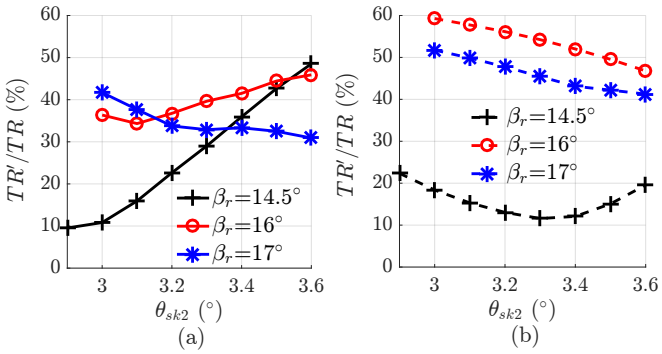

Fig. 12. Ratio of torque ripple in a skewed machine to torque ripple in an un-skewed machine when it is (a) non-saturated and (b) saturated.

A. *Effect of the method for non-saturated machines*

Similar to the analysis in section III, this method is analyzed for different situations. The selection of θ_{sk2} should consider the relationship between torque components. For dominant T_{ff6} or $T_{f,ph6}$, θ_{sk2} should be selected to minimize $\hat{L}_{f6}$ or $\hat{M}_{fa5}$, respectively. Based on 2D FEA, the influence of θ_{sk2} on $\hat{L}_{f6}$ and $\hat{M}_{fa5}$ is given in Fig. 11. As a result, minimization of the torque ripple is reached when θ_{sk2} is close to 2.9° and 3.6° for $\beta_r = 14.5°$ and $\beta_r = 17°$, respectively. This is verified by the torque ripple shown in Fig. 12(a). Additionally, the ratio of average torque in a skewed machine to average torque in an un-skewed machine is shown in Fig. 13(a).

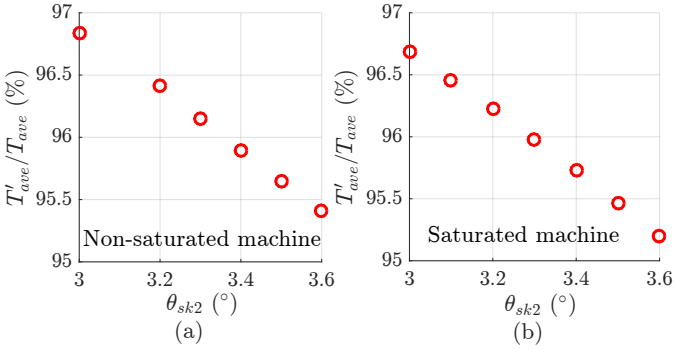

Fig. 13. Ratio of average torque in a skewed machine to average torque in an un-skewed machine ($\beta_r = 16°$) when it is (a) non-saturated and (b) saturated.

B. *Effect of the method for saturated machines*

If the machine is saturated, the influence of θ_{sk2} on torque ripple and average torque is shown in Fig. 12(b) and Fig. 13(b), respectively. As a result, the torque ripple is affected significantly by saturation while the average torque is not.

Above all, the selection of skewing angle is of crucial importance for torque ripple reduction. The effect of the two methods is similar in both non-saturated and saturated machines. The torque ripple is reduced at least 50% for different situations with an average torque reduction no more than 5%.

V. Conclusion

In this paper, methods of stepped rotor skewing and rotor teeth non-uniformity are analyzed for 12/10 VFRMs. The analysis of torque ripple shows significant contributions from T_{ff} and $T_{f,ph}$. The relationship between these two torque components strongly influences the selection of the skewing angle. In addition, saturation has a significant impact on the relationship between torque ripple reduction and skewing angle, while the average torque is almost not affected. Above all, the effectiveness of the two methods is similar. By properly selecting the skewing angle, the torque ripple is at least reduced by 50% with no more than 5% average torque reduction.

References

[1] J. Bao and K. Boynov, J.J.H. Paulides, K. Wijnands and E.A. Lomonova *Comparison of 48V rare-earth-free reluctance traction motor drives for mild hybrid powertrain*, VPPC, pp. 1-6, 2016.

[2] Z.Q. Zhu and X. Liu *Novel stator electrically field excited synchronous machines without rare-earth magnet*, IEEE Trans. on magnetics, vol. 51, no. 4, pp. 1-9, 2015.

[3] S. Jia, R. Qu and J. Li *Design considerations and parameter optimization of stator wound field synchronous machines based on magnetic the gear effect*, Proc. ECCE, pp. 5195-5202, 2015.

[4] B. Lee and Z.Q. Zhu *Torque ripple reduction for 6-stator/4-rotor-pole variable flux reluctance machines by using harmonic field current injection*, ECCE, pp. 1-8, 2016.

[5] M. Lin, R. Qu, J. Li, S. Jia and Y. Lu *Torque ripple reduction techniques for stator DC winding excited vernier reluctance machines*, ECCE, pp. 1-8, 2016.

[6] Y. Ueda, H. Takahashi, T. Akiba and M. Yoshida, *Small Cogging-torque transverse-flux motor with magnetic short circuit under unloaded condition*, in IEEE Trans. on Magnetics, vol. 50, no. 11, pp. 1-4, Nov. 2014.

[7] Y. Tang, J.J.H. Paulides and E.A. Lomonova, *Energy conversion in DC excited flux-switching machines*, in IEEE Trans. on Magnetics, vol. 50, no. 11, pp. 1-4, Nov. 2014.

[8] W. Fei, P.C Luk and Wen. Liang, *Comparison of torque characteristics in permanent magnet synchronous machine with conventional and herringbone rotor step skewing techniques*, in ECCE, pp. 1-8, 2016.

[9] X.B. Bomela and M.J. Kamper, *Effect of stator chording and rotor skewing on performance of reluctance synchronous machine*, IEEE Trans. on Industry Applications, vol. 38, no. 1, pp. 91-100, 2002.